NEUROSCIENCE

Activity of a direct VTA to ventral pallidum GABA pathway encodes unconditioned reward value and sustains motivation for reward

Wen-Liang Zhou[1], Kristen Kim[2], Farhan Ali[1], Steven T. Pittenger[1], Cali A. Calarco[2]†, Yann S. Mineur[1], Charu Ramakrishnan[3], Karl Deisseroth[3], Alex C. Kwan[1], Marina R. Picciotto[1,4]*

Dopamine signaling from the ventral tegmental area (VTA) plays critical roles in reward-related behaviors, but less is known about the functions of neighboring VTA GABAergic neurons. We show here that a primary target of VTA GABA projection neurons is the ventral pallidum (VP). Activity of VTA-to-VP–projecting GABA neurons correlates consistently with size and palatability of the reward and does not change following cue learning, providing a direct measure of reward value. Chemogenetic stimulation of this GABA projection increased activity of a subset of VP neurons that were active while mice were seeking reward. Optogenetic stimulation of this pathway improved performance in a cue-reward task and maintained motivation to work for reward over days. This VTA GABA projection provides information about reward value directly to the VP, likely distinct from the prediction error signal carried by VTA dopamine neurons.

INTRODUCTION

The ventral tegmental area (VTA) plays a central role in reward-motivated behaviors. Within the VTA, dopaminergic (DA) neurons have been thought to be the principal cells responsible for mediating reward-related behaviors (*1*), encoding reward prediction error signals (*2*), and promoting motivation to obtain rewards (*3*). Nevertheless, recent studies have increasingly documented γ-aminobutyric acid (GABA)–dependent functions of the VTA (*4*–*6*). For example, activity of VTA GABAergic neurons can signal an expected reward, which is necessary for DA neurons to calculate prediction error (*7*). VTA GABA neurons can modulate some forms of learning through control of DA and cholinergic systems (*8*) and pause nucleus accumbens (NAc) cholinergic interneuron firing to enhance associative learning (*9*, *10*). GABA neuron firing in the VTA increases before intracranial self-stimulation (*11*) and during arousal (*12*), which are closely associated with reward-motivated behaviors (*13*).

There are multiple subtypes of GABA neurons within the VTA, including a large population of locally projecting interneurons. GABA neurons comprise from 12 to 45% of neurons in different subnuclei of the VTA (*14*). Stimulation of all VTA GABA neurons disrupts reward consumption (*15*) and drives conditioned place aversion (*16*) by inhibiting neighboring DA neurons, whereas genetic inhibition or lesion of VTA GABA neurons causes sustained wakefulness and mania-like behaviors (*17*, *18*). While most of these functions of VTA GABA neurons have been attributed to local interneurons (*19*), it is becoming increasingly evident that different populations of GABA projection neurons contribute to reward-related behaviors, including projections to the NAc and lateral habenula (*9*, *10*, *20*). GABA is also co-released by a subset of VTA glutamatergic projection neurons, and stimulating these neurons is reinforcing (*21*). The dense GABAergic projection from the VTA to the ventral pallidum (VP) (*20*) is of particular interest because the VP, particularly the posterior VP, receives substantial GABA projections from the NAc that can be stimulated or inhibited as a result of VTA DA release via D1 or D2 receptors (*22*, *23*) and because the VP is the major output of mesolimbic system. Thus, in contrast to local VTA GABA interneurons, which decrease the effects of DA neuron signaling, we hypothesize that VTA GABA projections to the posterior VP, an area known to be involved in reward and motivation (*24*), could mimic or even potentiate behaviors dependent on DA signaling.

In this study, we show that VTA GABA projection neurons form functional synapses on GABAergic, cholinergic, and CaMK2α-expressing neurons of the VP unlike the selective cholinergic targets of the VTA-to-NAc projection (*9*, *10*). Unexpectedly, fiber photometry recording revealed that these neurons respond consistently to a primary, unconditioned reward and that the magnitude of this response is positively correlated with size and palatability of the reward. The response of this pathway to primary reward is relatively invariant and does not change in magnitude as animals learn that a cue predicts reward availability. In vivo single-cell calcium imaging in head-fixed mice in a sucrose-seeking task reveals that VP neurons respond to both reward seeking–associated motor activity and reward consumption. Selective chemogenetic stimulation of the VTA-to-VP GABA pathway significantly increased the fraction of VP neurons responsive to reward-motivated motor activity but not those to reward consumption. Optogenetic stimulation of these neurons in freely moving mice demonstrates that stimulating this projection enhances performance in a cued reward task (CRT) and maintains high motivation for reward during a progressive ratio (PR) schedule of reinforcement across multiple days. Together, these experiments identify a stable signal that scales with the value of a primary reward and potentiates learning of reward-related tasks but does not shift during cue learning.

[1]Department of Psychiatry, Yale University, 34 Park Street, New Haven, CT 06508, USA. [2]Interdepartmental Neuroscience Program, Yale School of Medicine, New Haven, CT 06520, USA. [3]Department of Bioengineering, Stanford University, Stanford, CA 94305, USA. [4]Kavli Institute for Neuroscience, Yale School of Medicine, New Haven, CT 06520, USA.
*Corresponding author. Email: marina.picciotto@yale.edu
†Present address: Department of Anatomy and Neurobiology, University of Maryland School of Medicine, Baltimore, MD 21201, USA.

RESULTS

VTA GABA neurons project to the VP and make synaptic connections with VP resident cells

To identify the most abundant postsynaptic targets of VTA GABAergic axons, we first infused an Adeno-associated virus (AAV) carrying a Cre-dependent construct (AAV2-EF1a-DIO-hChR2-eYFP) into the VTA of GAD65-Cre mice that labels GAD$^+$ neurons with enhanced yellow fluorescent protein (eYFP) (Fig. 1A and fig. S1A). eYFP-expressing VTA GABAergic axons densely innervated the basal forebrain, terminating abundantly in the VP (Fig. 1B), forming terminal structures (fig. S3A). We labeled postsynaptic VP neurons with a biocytin–Alexa Fluor 594 conjugate and found that eYFP$^+$ axons from VTA physically wrapped the cell body and proximal dendrites of the connected VP neurons (Fig. 1C).

There are multiple neuronal subtypes in the VP, with a large component of GABA cells comprising the primary output neurons of the structure (*25*). Previous studies have shown that functional VTA-to-NAc GABA projections activate cholinergic neurons selectively (*9*, *10*). Therefore, we infused a recombinant herpes simplex virus (HSV; H129ΔTK-TT) to label synaptically connected target cells of VTA-to-VP GAD$^+$ neurons and then determined the subtypes of these postsynaptic cells. H129ΔTK-TT is activated to express tdTomato (tdT) exclusively in cells expressing Cre recombinase (GAD$^+$ neurons in VTA). The virus then travels anterogradely across synapses to label the postsynaptic target cells with tdT, demonstrating synaptic connections between VTA GAD$^+$ neurons and target cells in the VP (*26*). Transgenic expression of green fluorescent protein (GFP) in GAD67$^+$ cells allowed for identification of GABA neurons postsynaptically in VP. H129ΔTK-TT was infused into the VTA of double transgenic GAD65-Cre/GAD67-GFP mice (Fig. 1D and fig. S1B). VTA neurons were efficiently infected with the virus and expressed tdT 96 hours after viral infusion (figs. S1F and S3B). Of 203 postsynaptic tdT$^+$ neurons in VP, 122 (60%) were GAD67-GFP$^+$ and 8 (4%) were ChAT$^+$ (Fig. 1, E and G). In separate slices, we observed that 6 of 104 (6%) infected VP neurons were CaMK2α$^+$ (Fig. 1, F and G). Thus, unlike what has been reported in the NAc, VTA GABA neurons not only predominantly make synaptic connections with GABA neurons in the VP but also target cholinergic and CaMK2α-expressing (potentially glutamatergic) VP neurons.

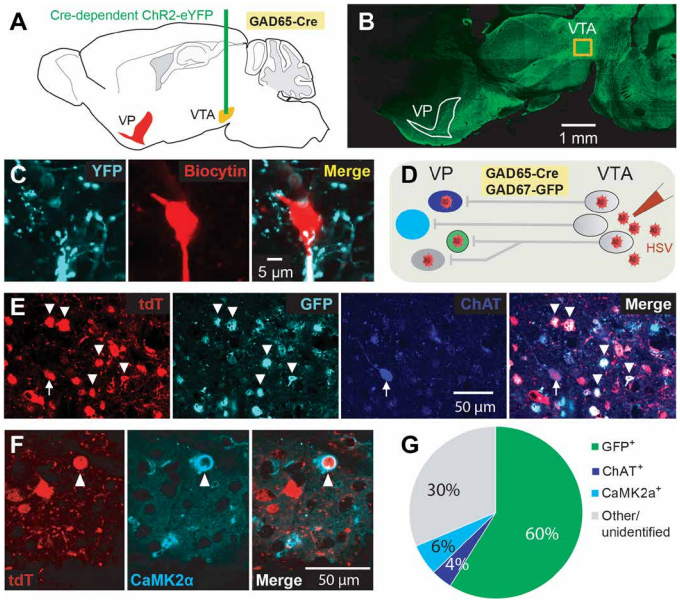

Fig. 1. VTA GABAergic neurons send long axons to the VP and form synaptic contacts with VP resident neurons. (**A**) Injection of AAV2-EF1a-DIO-hChR2-eYFP into the VTA of GAD65-Cre mice. (**B**) Sagittal view of a mouse brain expressing eYFP in VTA GAD65$^+$ neurons. The green fibers show the VTA GABA projection pathways. (**C**) Brain slices were cut from the mice treated as in (A), and a VP cell was then filled with biocytin and stained with Alexa Fluor 594. Images show that eYFP-expressing axons from VTA GAD65$^+$ neurons wrap the cell body and a proximal dendrite of the VP neuron. (**D**) Diagram for infection of H129ΔTK-TT into the VTA of GAD67-GFP/GAD65-Cre mice. The HSV construct is activated by Cre recombinase and transports viral replicates to connected postsynaptic neurons in the VP. (**E**) Confocal images taken from the VP, depicting postsynaptic targets of VTA GAD65$^+$ neurons infected by H129ΔTK-TT. tdT, GFP, and ChAT immunoreactivities denote HSV-infected, GAD67$^+$, and cholinergic neurons, respectively. Merged image shows colocalization of tdT with the molecular tags for identifying postsynaptic GABAergic and cholinergic neurons. (**F**) Images depicting colocalization of tdT with CaMK2α labeling in the VP. (**G**) Percentage of different subtypes of VP resident neurons postsynaptic to VTA GABAergic inputs.

Functional connections in VP: Electrophysiological evidence and characterization

To determine whether the connections of VTA GABAergic axons with VP neurons are functional, we performed whole-cell patch-clamp recordings in acute brain slices while optically stimulating ChR2-expressing VTA GABAergic axon terminals. In 31 VP neurons, we detected pronounced light-evoked postsynaptic currents (PSCs) (Fig. 2, A and B), including 5 neurons (from five different mice) recorded with tetrodotoxin (0.5 μM) in the bath, confirming monosynaptic transmission. The current size ranged from 10 to several hundred picoamperes (Fig. 2C), with a synaptic delay of 2 to 8 ms (Fig. 2D). On the basis of the intrinsic property of spike accommodation [reduction of a neuron's firing rate to a stimulus of constant intensity (*27*)], which plays an important role in neural coding, we categorized these recorded postsynaptic neurons into spike accommodation (Fig. 2E, blue circles, and fig. S4B2) and non-spike accommodation neurons (Fig. 2E, red circles, and fig. S4B1). In 4 of 17 non-spike accommodation neurons, we observed marked H-current (fig. S4B1, bottom), which modulates intrinsic rhythmicity.

To confirm that GAD65$^+$ terminals in the VP release GABA and evoke inhibitory PSCs, we applied picrotoxin (PTX; 100 μM) to block GABA type A ($GABA_A$) receptor–dependent responses. In 8 of 11 VP neurons, PTX nearly completely blocked PSCs (Fig. 2, A and F). However, in an additional three neurons (non-spike accommodation), PTX alone did not abolish the PSCs at a concentration as high as 500 μM but reduced the amplitude from −205 to −130 pA on average. Addition of 6-cyano-7-nitroquinoxaline-2,3-dione (CNQX) suppressed the remaining component of these PSCs (Fig. 2, B and F). This indicates that a subset of VTA GABA projections may release glutamate, consistent with reports that some VTA GAD$^+$ neurons release both GABA and glutamate in the lateral habenula (LHb) and the dentate gyrus (*28*, *29*), and that VTA VGluT2$^+$ neurons co-release GABA in LHb and VP (*21*, *28*).

Activity of VTA-to-VP GABA neurons scales with size and palatability of the unconditioned reward

VTA GABA neurons have been shown to increase their firing in response to reward-related stimuli and arousal (*11*, *12*). To determine whether the activity of VTA-to-VP GABA neurons is recruited during reward-related behaviors, we designed three tasks to examine

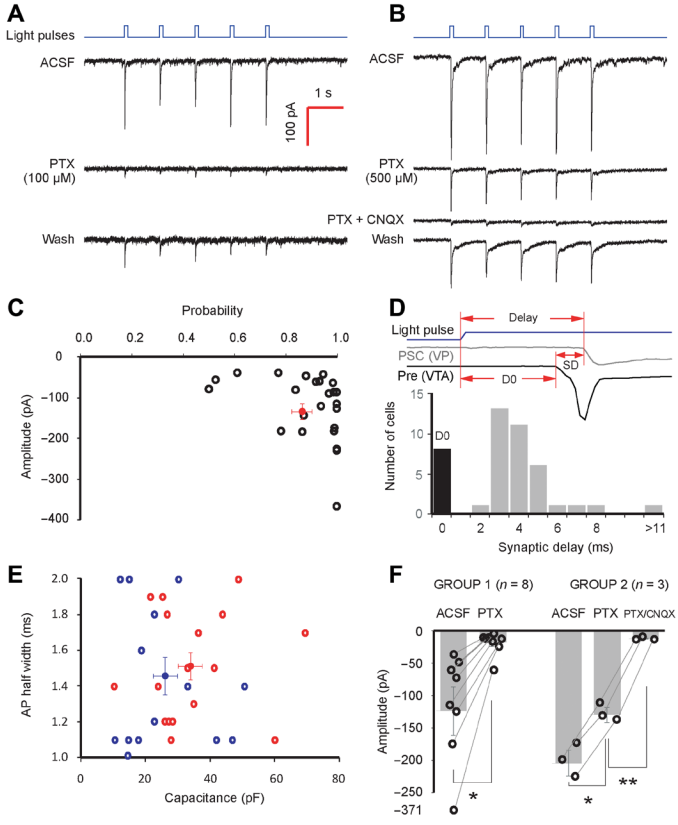

Fig. 2. Optical stimulation of VTA-to-VP GABAergic axon terminals evokes postsynaptic currents (PSCs) in VP neurons. (**A**) Example traces from whole-cell patch-clamp recordings in a VP neuron. The brain slice was from a mouse treated as in Fig. 1A. Upper blue line indicates blue light pulses. (**B**) Same as (A) except that PTX was applied at 500 μM, and 10 μM CNQX was added to fully suppress light-evoked currents. (**C**) Characterization of light-evoked PSCs, current amplitude versus probability plot. The red dot denotes the average current size and probability (mean ± SE, apply to all figures). Probability = number of detectable evoked synaptic responses/number of stimulus light pulses. (**D**) Upper panel shows the measure of synaptic delay (SD). The gray trace was recorded in a postsynaptic VP neuron, and the black trace was recorded in a ChR2-expressing VTA neuron. The delay in the black trace (D0) was considered to be a systematic delay. In the lower panel, the black bar corrects the systematic delay recorded in presynaptic ChR2-expressing cells (8.5 ms) to 0; gray bars show corrected synaptic delay in postsynaptic VP neurons. (**E**) Characterization of action potential half-width versus cell capacitance plot in postsynaptic VP neurons. Red circles denote cells showing a continuous firing pattern (fig. S4B1), and blue circles denote cells exhibiting marked spike accommodation (fig. S4B2). The red and blue dots denote the average of the two groups. (**F**) Composition of light-evoked PSCs. In group 1, the PSCs were blocked by PTX. Addition of CNQX resulted in no further significant changes. In group 2, the PSCs were blocked by a combination of PTX and CNQX. Student's *t* test, $^{*}P < 0.05$; $^{**}P < 0.01$.

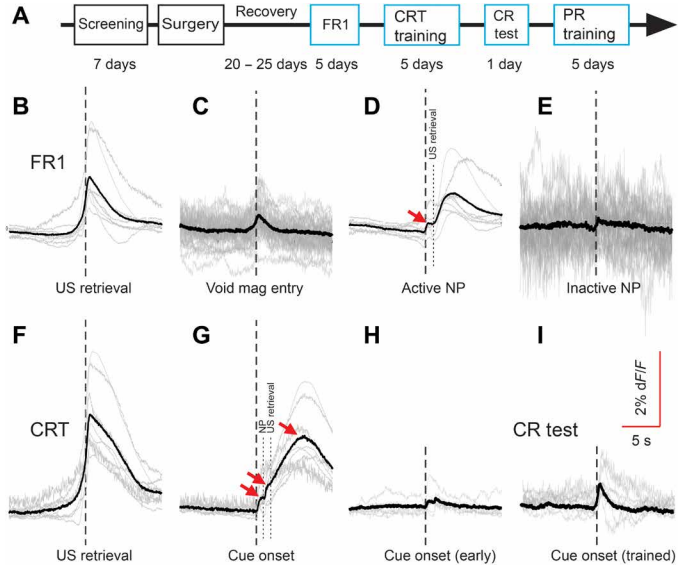

Fig. 3. Activity of VTA-to-VP GABA neurons during rewarded behaviors. (**A**) Timeline of behavioral procedures and fiber photometry sessions (blue boxes). (**B**) Fluorescence changes (d*F*/*F*) during FR1 responding. Signals were aligned to US retrieval [black dashed lines in (B) to (I) indicate timing of the events to which the signals were aligned]. Black trace represents the averaged result; gray traces in (B), (D), (F), and (G) represent averaged signals in each individual mouse. *N* = 8 mice. (**C**) Fluorescence signals when mice visited the magazine when no reward was available. Gray traces in (C), (E), (H), and (I) represent signals to each reward event. (**D**) Same as (B) except signals were aligned to active nosepokes. (**E**) Fluorescence signals when mice made inactive nosepokes. (**F**) Fluorescence changes during CRT training. Signals were aligned to US retrieval. (**G**) Same as (F) except signals were aligned to the onset of tones. The dashed lines marked "NP" and "US retrieval" show the timing of nosepoke and magazine entry following the corresponding tones. Red arrows indicate the signal following the three behavioral events: tone, nosepoke, and US retrieval. (**H**) Signals when mice received tones in the beginning of the first CRT session before any reward was presented. (**I**) Signals during conditioned reinforcement (CR) testing when mice received tones alone.

different aspects of unconditioned and learned reward responses, including a non-cued fixed-ratio operant task, a cued reward operant learning task (CRT) to measure cue-reward learning, and a PR responding task to evaluate motivation to work for rewards (Fig. 3A). We then used fiber photometry to record in vivo calcium levels from VTA GABAergic axon terminals in VP across all behavioral phases as a measure of neuronal activity. To record activity from VTA-to-VP GABA terminals selectively, we injected pGP-AAV1-syn-FLEX-jGCaMP7s-WPRE into the VTA of GAD65-Cre mice and implanted an optical fiber targeting the VP. This allowed us to record calcium-dependent fluorescence signals from the terminals of VTA GAD^{+} neurons in the VP of behaving mice (fig. S1, C and G). During fixed-ratio 1 (FR1) responding for reward, a fluorescence transient (2.06 ± 0.31%, *n* = 8 mice) peaked ~0.5 s after the animal visited the magazine in which reward was delivered (US retrieval) (Fig. 3B). A magazine entry made when no reward was present triggered a much smaller signal (0.45%; Fig. 3C). To determine whether the transient occurred exclusively in response to the primary reinforcer, we aligned the same signal to the nosepoke that triggered the reward. We observed a smaller peak (~0.3%, arrow; Fig. 3D) within 0.5 s following the nosepoke and preceding US retrieval, although the steepest increase with greatest magnitude occurred after US retrieval. Inactive nosepokes resulted in only very small blips in fluorescence (Fig. 3E), indicating that the activity of these neurons was correlated with US retrieval and/or consumption.

We next recorded activity of VTA-to-VP GABA terminals during a CRT, in which animals learned that a tone (cue, as an occasion setter) predicted availability of the reward. The tone was presented on average every 30 s with a random time interval (RT-30 schedule). A nosepoke in the active aperture within 5 s following the tone resulted in delivery of the primary reinforcer. We measured pronounced fluorescent transients in VTA-to-VP GABA neurons that

peaked ~0.5 s following US retrieval (2.87 ± 0.45%; Fig. 3F), which were consistent across all five consecutive sessions, up to 150 trials (Fig. 4, A and B). We next aligned the same signals to the tone (Fig. 3G) and averaged the timing of nosepokes and US retrievals to identify three different phases in the signal. The largest response was invariably observed during US retrieval and did not change across sessions. In contrast, at the beginning of the first CRT session before any reward had been presented, there was no notable transient during delivery of the tone (Fig. 3H); however, after CRT training, the cue induced a small but discernible fluorescence signal (Fig. 3G, indicated with the first arrow), likely reflecting the acquired reward value of the tone. Consistent with this possibility, when mice learned to perform an previously unexposed operant task to obtain cue delivery in the absence of the primary reinforcer [conditioned reinforcement (CR)], the tone alone resulted in a small but discernible fluorescence response (0.83 ± 0.09%, Fig. 3I).

To determine whether the effort required to obtain a reward might alter the response of VTA-to-VP GABA neurons, we measured fluorescence over 5 days of PR responding. US retrieval–associated fluorescence transients were observed consistently across all trials, and all five sessions did not change as effort demands increased or breakpoints were reached (figs. S5 and S6).

VTA DA neurons signal a reward prediction error, first firing to an unconditioned reward, then shifting to a reward-predictive cue following multiple training trials, and no longer signaling the primary reward. To calculate prediction error, there must be an additional neuronal signal encoding the value of the primary reward. Neuronal signals for reward have been recorded in the VTA (*7*), but the identity of the neuronal subtype encoding an invariant signal for an unconditioned reward is not known. Therefore, we next tested whether activity of VTA-to-VP GABA neurons encodes the value of an unconditioned reward. First, mice were tested on FR1 responding for various size rewards. Each nosepoke triggered reward delivery for 0 (no reward), 1, 2, 3, 4, or 5 s, randomly. The peak signal amplitude in response to different reward sizes did not change significantly (Fig. 4, C and D, top); however, the area under the curve (AUC) from 0 to 5 s after US retrieval increased significantly with increasing reward size (Fig. 4D, bottom). In a second experiment, mice were tested on FR1 responding for the same volume (2-s delivery) of reward, but Ensure was diluted with water at 1:1 (the dilution used for all other experiments), 1:3, 1;10, 1:50, and 0 (water) to vary palatability. The size of the fluorescence signals in VTA-to-VP GABA terminals was notably correlated with the dilution of reward (Fig. 4, E and F) and did not vary across the session, suggesting that the signal did not change as animals became sated. These experiments indicate that the activity of the VTA-to-VP GABA pathway can provide stable information on the magnitude of a rewarding stimulus.

Together, these data demonstrate that VTA-to-VP GABA neurons increase activity in response to retrieval/consumption of an unconditioned reward. The response to primary reward does not decrease (or increase) following cue-reward learning; however, stimuli (cues) that acquire rewarding properties as a result of learning can subsequently elicit small responses in these neurons. Activity of VTA-to-VP GABA neurons therefore appears to encode the value of a reward, reflecting the size and, more remarkably, the palatability of a reward.

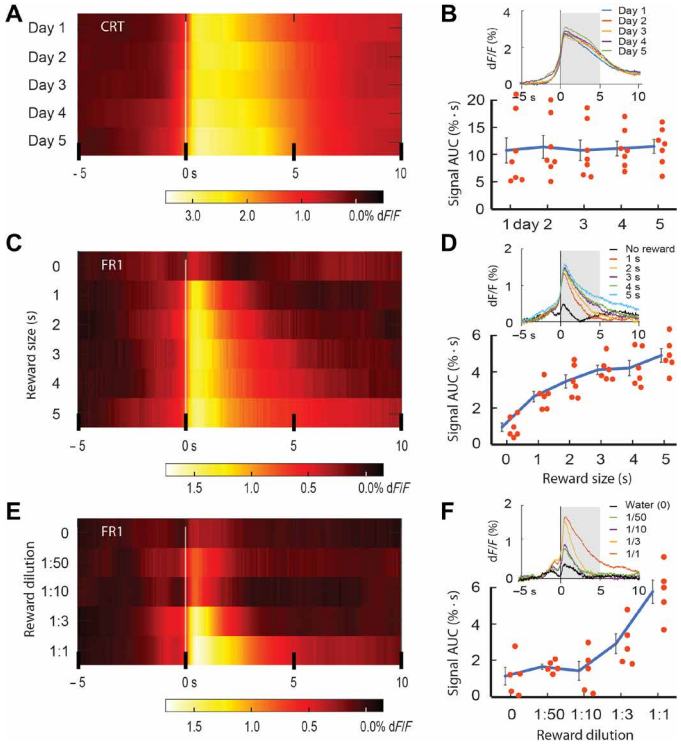

Fig. 4. Activity of the VTA-to-VP GABA pathway scales with the value of a primary reward. (**A**) Heatmap of calcium-dependent fluorescence signals in VTA-to-VP GABA neurons across five CRT sessions on consecutive days. Signals were aligned to the time of magazine entry (0 s). (**B**) Area under the curve (AUC) of fluorescence signals measured from (A). Upper panel shows the fluorescence change across five sessions. Lower panel shows the AUCs calculated from the upper panel curves from 0 to 5 s (gray area). Each dot represents the averaged AUC of the fluorescence signals measured in one mouse in one session. One-way analysis of variance (ANOVA) of the signal AUC across five sessions: $F_{(4,30)} = 0.034$; $P = 0.998$. $N = 7$ mice. (**C**) Heatmap of fluorescence signals in terminals of VTA-to-VP GABA neurons during FR1 responding to different sizes of reward (reward delivery for 0, 1, 2, 3, 4, and 5 s). (**D**) AUC of fluorescence signals measured from (C). Upper panel shows the fluorescence change in response to different sizes of reward. Lower panel shows the AUCs calculated from the upper panel curves. One-way ANOVA of the signal AUC across reward sizes: $F_{(5,30)} = 18.6$; $P = 2.2 \times 10^{-8}$. $N = 6$ mice. (**E**) Heatmap of fluorescence signals in VTA-to-VP GABA neurons during FR1 responding to different dilutions of reward with the same reward delivery for 2 s. (**F**) AUC of fluorescence signals measured from (E). Upper panel shows the fluorescence change in response to different dilutions of reward. Lower panel shows the AUCs calculated from the upper panel curves. One-way ANOVA of the signal AUC across different dilutions: $F_{(4,20)} = 14.7$; $P = 9.4 \times 10^{-6}$. $N = 5$ mice.

VP neuronal activity increases in response to motivated motor activity and is modulated by VTA-to-VP GABA pathway

VP neurons are known to respond to reward and to encode incentive value and internal drive (*30*, *31*). We therefore postulated that direct VTA GABA projections that are activated by reward might be important in altering the activity of the overall VP network. We designed an intersectional chemogenetic strategy to stimulate the VTA-to-VP GABAergic pathway selectively while mice performed a self-paced, instrumental sucrose-seeking task (*32*) and combined this motivated reward seeking with in vivo single-cell calcium imaging. In this chemogenetic strategy, a Cre-dependent Flp recombinase construct packaged into a retrograde HSV is infused into the VP of GAD-Cre mice. All axon terminals in the VP can take up the

retrograde virus, but the Cre-dependent Flp construct is only expressed in GAD$^+$ cell bodies. The Flp-dependent Gq-DREADD construct is infused into the VTA of the same animals. This assures that Gq-DREADD is expressed exclusively in the VP-projecting VTA GAD$^+$ neurons (Fig. 5, A and B, and fig. S8). In addition, the calcium indicator GCaMP6s is expressed in all VP neuronal subtypes under control of the synapsin promoter, so the consequences of stimulating VTA-to-VP GABA neurons can be recorded.

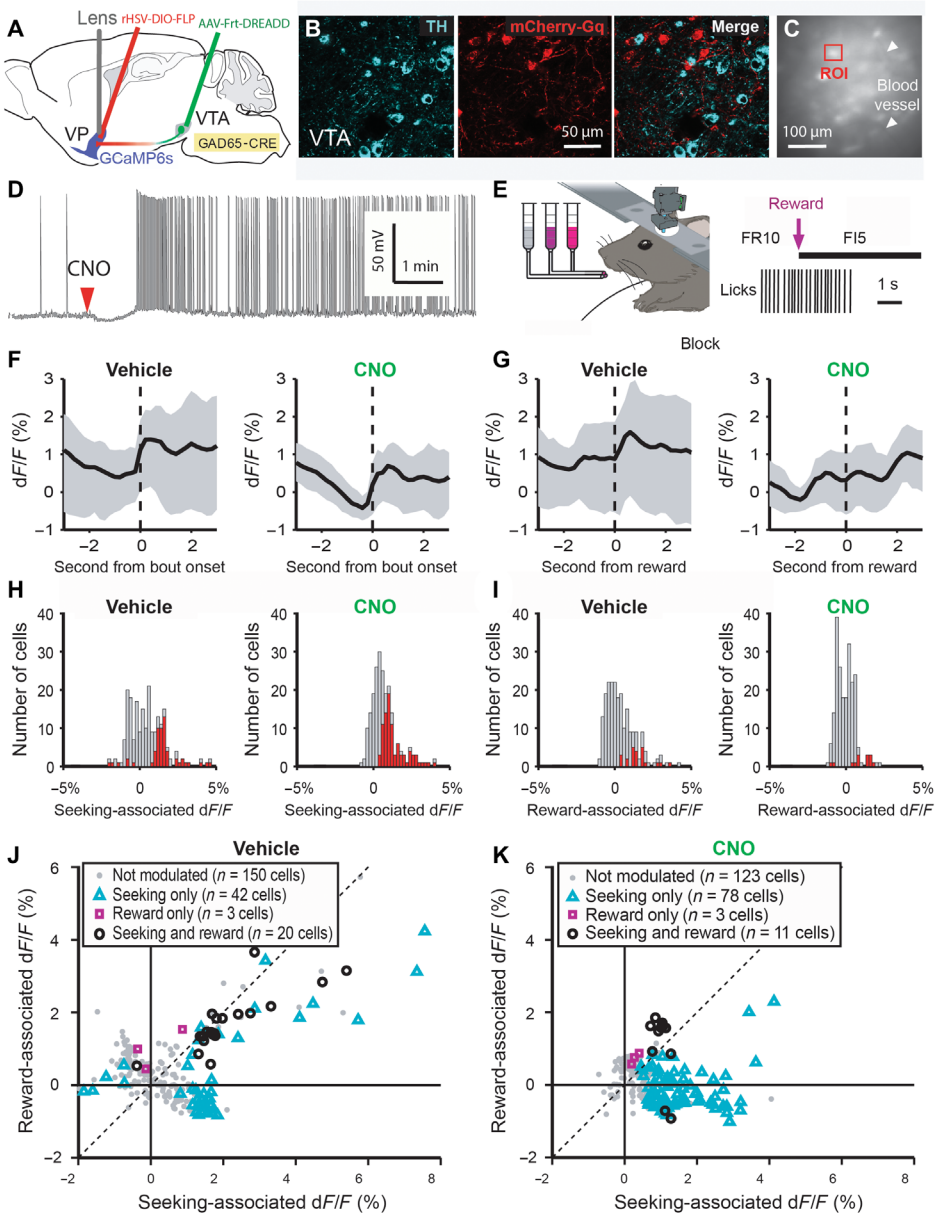

Fig. 5. Stimulation of VTA-to-VP GABA pathway modulates VP activity during reward seeking. (**A**) Intersectional strategy targeting Gq-DREADD to VTA-to-VP GABA projections and recording in VP. Gray line, placement of lens. Syn1-GCaMP6s (blue) was expressed in VP for recording from all neuronal subtypes. Retrograde AAV carrying Cre-dependent Flp (rHSV-DIO-flp) was injected into VP of the same GAD65-Cre mice to express Flp recombinase in Cre-expressing neurons with terminals in VP. Last, Flp-dependent Gq-DREADD (AAV-Frt-DREADD) was injected into the VTA, allowing expression of the DREADD only in GAD$^+$ VTA neurons with terminals in VP that had taken up the Flp construct. (**B**) VTA tyrosine hydroxylase (TH) and mCherry staining in a GAD65-Cre mouse with AAV8-Ef1a-fDIO-DREADD Gq-mCherry and VP:rHSV-hEF1α-LS1L-flpo. The DREADD is not expressed in TH$^+$ cell bodies. (**C**) Frame taken through the microscope in VP showing neurons expressing GCaMP6s. (**D**) Whole-cell patch-clamp recording of Gq-DREADD-mCherry+ VTA neuron. Red arrowhead indicates the time when CNO (10 μM) was added. (**E**) Scheme for head-fixed sucrose seeking. Rewards earned on an FR10-FI5 schedule (right). (**F**) Fluorescence changes (d*F*/*F*) aligned to onset of each lick bout. Black lines indicate averages of the transients; gray shading indicates 20 to 80% of individual traces. *N* = 3 mice. (**G**) Fluorescence changes aligned to time of reward delivery. (**H** and **I**) Distribution of event-associated fluorescence changes. (H) Transients aligned to onset of "seeking" lick bout (vehicle versus CNO, $P = 0.0008$, χ^2 test). (I) Transients aligned to liquid delivery (vehicle versus CNO, $P = 0.0524$, χ^2 test). All cells had been examined using the Wilcoxon signed-rank test, pre-event d*F*/*F* versus post-event d*F*/*F*. Cells with no significant changes ($P \geq 0.05$, gray bars) and cells with significant changes ($P < 0.05$, red bars) were grouped. (**J** and **K**) Scatterplot of individual neuron responses at time of reward seeking versus consumption after (J) vehicle or (K) CNO (Wilcoxon signed-rank test, pre-event versus post-event).

For in vivo calcium imaging, tri-viral (VP:GCaMP6s + rDIO-Flp/VTA:fDIO-DREADD) infected GAD65-Cre mice ($n = 3$) were trained in a head-fixed paradigm to seek fluid by licking a spout on a fixed-ratio 10, fixed-interval 5 (FR10-FI5) schedule in which 10 licks resulted in a reward delivery with 5 s between periods of reward availability (Fig. 5E). Water (0%) and sucrose (3 and 10%) solutions were delivered separately as rewards during each 60-s time block, which is initiated by completing the first FR10 lick bout. To record VP neuronal activity, a lens targeting the posterior VP virus injection site was implanted (fig. S9). Consumption of solutions decreased after the first eight blocks of each session, so we analyzed these eight blocks together to exclude effects of satiation and depletion of terminal GABA vesicles after excessive chemogenetic stimulation. Control mice (GAD65-Cre) received the DREADD construct in the VTA but no Flp construct in the VP. All mice were administered vehicle and then clozapine *N*-oxide (CNO) to ensure that there were no significant effects of CNO alone on neuronal activity or behavior in control mice (figs. S10 and S11). When calcium signals from VP neurons were aligned to the onset of a motivated lick bout, two distinct fluorescence transients were observed (Fig. 5, F and G). The first transient occurred around the time of action (licking) to obtain fluid delivery. Aligning the same data to the time of liquid delivery shows that the second transient occurred during reward consumption (Fig. 5G). DREADD-mediated activation of VTA-to-VP GABA neurons via CNO administration significantly increased the number of activated cells during reward seeking (41.4%, 89 of 215 cells; Fig. 5H and fig. S12C) compared to vehicle (26%, 56 of 215 cells; $P = 0.0008$, χ^2 test). Simultaneously, CNO tended to reduce the number of activated cells recruited during reward consumption (5.6%, 12 of 215 cells; Fig. 5I and fig. S12D) compared to vehicle (10.7%, 23 of 215 cells; $P = 0.052$, χ^2 test). These results indicate that a large proportion of VP neurons fire in response to an action that leads to reward delivery, consistent with a role in motivation to work for reward (*33*). Stimulating VTA-to-VP GABA neurons recruited more VP cells when the animals were working to obtain a reward and decreased the fraction of firing cells in VP during reward consumption. When animals were satiated with fluid, the effect of VTA-to-VP GABA stimulation was reversed (fig. S13). Analysis of individual cells reveals that most consumption-responsive cells are also active during reward seeking (Fig. 5, J and K, black circles), indicating that consumption-responsive neurons are largely recruited from those relevant to motivation. This experiment shows that activation of the VTA-to-VP GABA pathway increases the fraction of cells responsive to reward seeking, and not those responding to reward consumption alone (Fig. 5K). Combined with the relatively invariant response of the VTA-to-VP GABA neurons during US retrieval, these data suggest that the GABA input signals reward consumption, but then likely transmits information to the VP network that encodes the motivational aspects of the behavior.

Optogenetic stimulation of the VTA-to-VP GABA pathway enhances performance in CRT and non-CRT

Given that fiber photometry experiments demonstrated that the VTA-to-VP GABA neurons increase activity in response to primary rewards, and that in vivo calcium imaging during reward seeking suggests that stimulation of this pathway alters the VP network to respond preferentially to reward seeking, we hypothesized that the behavioral consequence of stimulating this input to the VP may contribute to increased motivation to work for rewards. We therefore screened mice for high responders for reward and then randomized mice to two groups (fig. S14) for infusion of AAV-EF1a-DIO-hChR2-eYFP (stimulation) or AAV-EF1a-DIO-eYFP (control) into the VTA (fig. S1, A and E) and implanted a light cannula targeting bilateral posterior VP (figs. S1, D and H, and S2) to manipulate the activity of this projection selectively in behaving mice. Self-stimulation of VTA-to-VP GABA projections does not maintain robust operant responding over multiple sessions (fig. S15), suggesting that it is not equivalent to behavior observed following stimulation of the medial forebrain bundle.

We next stimulated VTA GAD^+ neuronal terminals in the VP and evaluated performance in the same behavioral tasks used to measure activity of these neurons (Figs. 3 and 4). Similarly in CRT, a tone was presented to the mice on an RT-30 schedule, and immediately after the tone, a 5-s reward contingency window was assigned when a nosepoke in the active aperture resulted in delivery of a reinforcer. Fiber photometry results revealed that reward consumption reliably evokes activity in the VTA-to-VP GABA pathway (Fig. 3). After training, mice respond to the cue quickly with a nosepoke and then a magazine entry, usually within 2 s after onset of the cue, resulting in robust activity of VTA-to-VP GABA terminals (Fig. 3G). We therefore delivered a 5-s train of blue light pulses to the terminals of VTA-to-VP GAD^+ neurons during the reward contingency window immediately following tone presentation to induce phasic activity of the pathway in a pattern that might mimic reward consumption (*34*). This pattern of stimulation was intended to link phasic activity of the VTA-to-VP GAD^+ pathway to tone presentation. During the 5 days of CRT training (Fig. 6B), both "control" and "stimulated" animals learned to complete the task. However, ChR2-expressing mice performed significantly better than control animals in task completion time, effort conversion rate (number of reinforcers/total nosepokes), and acquisition rate (number of reinforcers/total tones; Fig. 6, C, F, and G). Following the 5-day training, we tested the associative strength of cue-reward pairing in each group in a previously unexposed CR task by allowing the mice to nosepoke for the cue alone (Fig. 6H). The ratio of nosepokes in the active versus inactive apertures was not significantly different between the two groups (Fig. 6I). Thus, while optogenetic stimulation accelerated learning to obtain rewards efficiently, once animals acquired the association, there was no difference in the associative strength of cue-reward pairing.

We hypothesized that improved performance in the CRT might reflect enhanced motivation to obtain the reward, rather than improved learning of the cue-reward contingency. PR schedules of reinforcement have been used widely to measure motivation for reward (*35*). We therefore tested whether stimulation of the VTA-to-VP GABA pathway affects behavior on a non-cued PR schedule. The same train of blue light pulses was delivered for 5 s at 30-s intervals across each PR session to stimulate VTA-to-VP GABA neurons, a pattern that could mimic receipt of additional rewards across the session. On the first day of PR testing, the two groups showed similar performance (Fig. 7), indicating that the stimulation did not alter motor activity or sensory processes compared to controls. However, on each successive PR session, the stimulated group sustained a high level of responding, reaching significantly higher breakpoints (number of responses required to obtain a reward), therefore earning more rewards than the control group (Fig. 7, A and B). We evaluated two factors contributing to total number of nosepokes: duration and frequency. Stimulation made the animals more persistent than

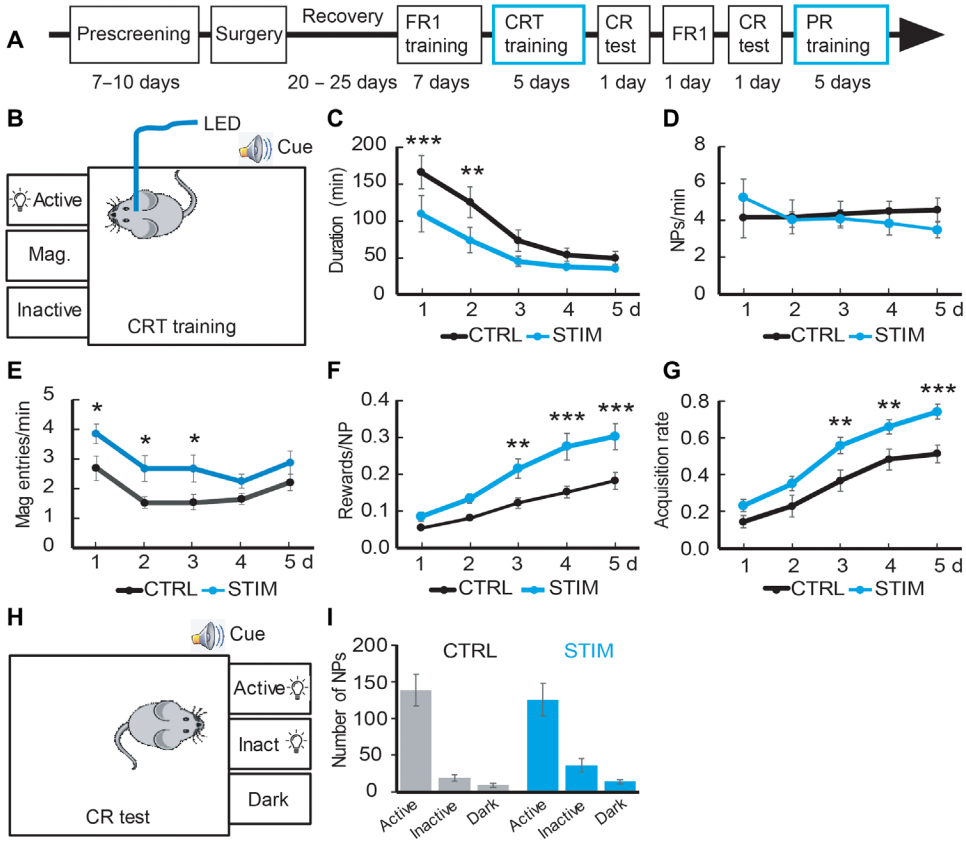

Fig. 6. Stimulation of VTA-to-VP GABA pathway improves performance in CRT. (**A**) Timeline of behavioral procedures and optical stimulation (blue boxes). (**B**) Settings of behavioral boxes used for CRT. (**C** to **G**) During CRT sessions, task duration [(C); $F_{(1,24)} = 7.65$, $P = 0.011$], nosepoke frequency [(D); $F_{(1,24)} = 0.073$, $P = 0.79$], magazine entry frequency [(E); $F_{(1,24)} = 6.20$, $P = 0.020$], effort conversion rates [number of reinforcers/total NPs; (F); $F_{(1,24)} = 17.79$, $P = 0.0003$], and reward acquisition rate [number of rewards/number of cues; (G); $F_{(1,24)} = 9.95$, $P = 0.0043$] were compared between control ($n = 13$) and "stimulation" ($n = 13$) groups. Two-way ANOVA was used to compare the two curves over 5 days. Uncorrected Fisher's least significant difference (LSD) was used for post hoc tests. *$P < 0.05$; **$P < 0.01$, ***$P < 0.001$. (**H**) Settings of boxes for CR tests. (**I**) Number of nosepokes in each aperture during the first CR test was compared between control ($n = 9$) and stimulation ($n = 8$) groups [two-way ANOVA: $F_{(1,15)} = 0.071$, $P = 0.794$].

the control group (Fig. 7C). While nosepoke frequency tended to be higher in the stimulated group, this did not reach significance (Fig. 7D). The increases in effort persistence and trial frequency both suggest that stimulation of the VTA-to-VP GABA pathway made mice more motivated to seek reward.

DISCUSSION

Salient stimuli increase activity of mesolimbic circuits, and this, in turn, can elicit reward-related behaviors. VTA DA neurons encode reward prediction error signals and convey this information primarily to the NAc, activating or inhibiting the direct (D1) and indirect (D2) pathways, respectively. In turn, both D1 and D2 medium spiny neurons (MSNs) from the NAc project densely to the VP (*25*). Rather than simply relaying reward information from mesolimbic to motor outputs, the VP integrates information from various sources (*20*, *36*–*40*), adding new information that allows the individual to adapt reward-related behavior appropriately to cues in the environment (*24*, *31*). Thus, the VP has been proposed to be an important "limbic final common pathway" for mesolimbic processing of rewards (*24*).

In this study, we found that dense VTA GABA inputs to the VP make synaptic connections with several classes of VP neurons, including GABAergic, cholinergic, CaMK2α-expressing, and possibly other cell types. This is in contrast to what has been reported for the connections that VTA GABA axons make in the neighboring NAc, where their postsynaptic targets are primarily cholinergic interneurons (*9*, *10*). Cholinergic pallidal neurons exhibit strong spike accommodation while noncholinergic neurons do not (*27*). On the basis of this classification, our electrophysiological results show that both cholinergic and noncholinergic VP neurons receive VTA GABA inputs. We also found that a subset of the axons derived from VTA GAD65$^+$ neurons released glutamate. GABA and glutamate co-release has been observed in other brain structures (*21*, *41*) and may partly explain why stimulation of VTA GAD65$^+$ neurons resulted in both inhibition and excitation of VP calcium activity during the self-paced sucrose-seeking task (fig. S12): Inhibition is caused by direct synaptic GABA transmission, while excitation could be caused by either disinhibition of local interneurons or glutamate release from GAD65$^+$ axonal terminals, shaping VP output to other limbic and motor systems necessary to act on reward-related information (*24*).

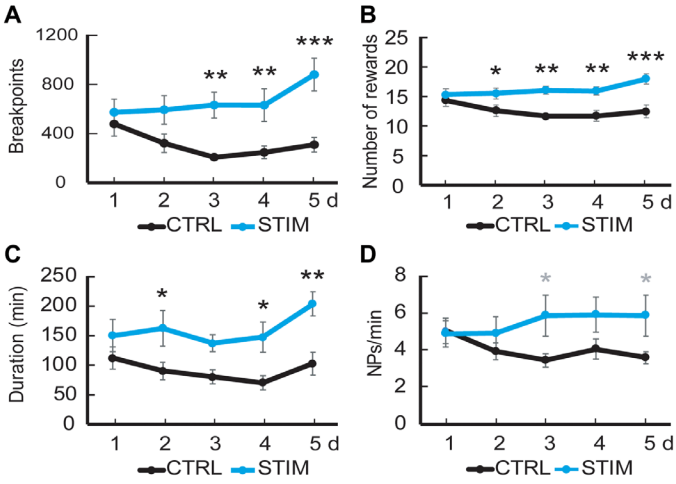

Fig. 7. Stimulation of VTA-to-VP GABA pathway increases motivation to obtain rewards in PR testing. Following CRT training and CR test as depicted in Fig. 6A, the mice were trained as in Fig. 6B on a PR schedule of reinforcement. Breakpoints [(**A**); $F_{(1,17)} = 9.23$, $P = 0.0074$], number of earned rewards [(**B**); $F_{(1,17)} = 11.83$, $P = 0.0031$], task duration [(**C**); $F_{(1,17)} = 13.5$, $P = 0.0019$], and nosepoke frequency [(**D**); $F_{(1,17)} = 2.36$, $P = 0.14$] were compared between control ($n = 10$) and stimulation ($n = 9$) groups. Two-way ANOVA compared the two curves over 5 days. Uncorrected Fisher's LSD was used for post hoc tests. *$P < 0.05$; **$P < 0.01$; ***$P < 0.001$.

We have shown that the activity of VTA-to-VP GABA neurons increased consistently in response to a primary reward, regardless of cue presentation, with a peak in calcium signals ~0.5 s following US retrieval. Similar to neighboring DA neurons, VTA-to-VP GABA projection neurons respond to the primary reward, and not to the cue, before training. In contrast, cue-reward training shifts the response of DA neurons to the cue as a prediction of reward delivery and eliminates the response to a predicted reward while decreasing response to an omitted reward as an error to the established prediction (*2*). VTA-to-VP GABA neurons also develop a response to a cue through cue-reward training but to a much lesser extent than is observed for DA neurons. Furthermore, the response to primary reward in VTA-to-VP GABA neurons seems not to change following prolonged cued reward training even when the animal has learned the association between the cue and the reward. This finding agrees with a previous report that VTA GABA neurons respond to the outcomes of behavioral events, not to cues (*42*). In the current study, we also performed PR testing and found that increased effort did not alter activity of this pathway in response to reward delivery, and we also did not see a decrease in activity of the VTA-to-VP GABA neurons following nosepokes that did not result in reward (Fig. 3E). The difference in patterns of activity between these two groups of VTA neurons likely reflects their different roles during reward behaviors. We hypothesize that VTA-to-VP GABA neurons may provide a mechanism to scale with the value of reward, allowing DA neurons to calculate the prediction error by comparing the predicted reward value, as reflected in DA neuron firing, and the current reward value, as encoded by VTA-to-VP GABA neurons. Target neurons in the VP are well positioned to relay information from VTA GABA projections to provide feedback to VTA DA neurons and to process and execute motivated behaviors (*25*). Recent studies show that manipulating the activity of a group of VP neurons can bidirectionally modulate motivation for reward seeking (*43*) and that activation of a group of NAc shell–projecting VP neurons promotes reward consumption (*44*). Therefore, we used an unlearned reward seeking/consumption paradigm to identify which neurons in the VP receive VTA-to-VP GABA inputs. A subset of VP neurons responded to the initiation of motor activity while the animal was working to obtain reward (seeking), and a smaller subset of neurons responded to consumption. The two cell populations overlapped, so only a small fraction of cells responded solely to consumption. Selective chemogenetic stimulation of the VTA-to-VP GABA pathway recruited more VP neurons to respond to reward seeking but did not modulate those cells responding to consumption alone. These results suggest that the VTA-to-VP GABA inputs may alter the VP network to encode motivational aspects of reward seeking.

The posterior VP targeted here is thought to be a "hedonic hotspot" (*24*). Opioid transmission in the hotspot enhances both "liking" and "wanting," while local blockade of $GABA_A$ transmission in the VP increased wanting but did not affect liking (*45*, *46*). Since VTA DA signaling can stimulate striatal D1 MSNs, some of which project to and release GABA in the VP (*22*, *23*), we hypothesized that direct VTA-to-VP GABA projections might be a synergistic pathway that provides a feedforward signal promoting motivated behaviors when the animal retrieves and consumes a reward. Consistent with this hypothesis, we found that selective optogenetic stimulation of VTA-to-VP GABA pathway resulted in significantly improved performance in a cued operant reward task, as well as significantly higher breakpoints and more earned rewards across 5 days of PR testing. These results support the idea that activity of the VTA-to-VP GABA pathway scales with the value of the primary reward and that this information is used by the VP to increase motivation to obtain the reward. Potentially, the increase in VTA-to-VP GABA activity in response to reward consumption recruits a larger set of VP neurons responsible for reward seeking, therefore increasing motivation to obtain a reward (or wanting) and promoting responding during reward-related tasks. On the other hand, DA signaling in striatum is essential for motivated behaviors (*47*), and there is another hedonic hotspot in the NAc shell that interacts with the VP as part of a larger neural network involved in reward seeking (*48*). The availability or consumption of a reward clearly triggers activity of both VTA DA and GABA neurons so that motivation to work for reward is orchestrated by these convergent VP circuits to allow the animal to complete behavioral tasks efficiently.

While it is likely that stimulation of these GAD^+ neurons leads to behavioral consequences as a result of GABA release, it is also possible that glutamate release contributes to the observed physiological and behavioral outcomes. The observation that a portion of the postsynaptic response in 3 of 11 VP cells recorded was not blocked by GABA antagonists but was blocked by CNQX suggests that co-release of glutamate could shape the physiological response to stimulation of these GAD^+ neurons. That said, the bulk of the postsynaptic responses to stimulation of the VTA to VP GAD^+ pathway could be blocked by $GABA_A$ antagonists, suggesting that GABA signaling is likely to be the primary mediator of the observed effects.

Recent studies have suggested that activity of VP GABAergic and glutamatergic neurons may represent internal states and can bias the direction of behavior toward either reward seeking or avoidance, respectively (*49*). Activation of VP GABA neurons potentiates reward seeking (*50*), while activity of VP glutamatergic neurons suppresses reward seeking (*51*). These functional studies fit well with

what is known about the inputs to these neurons from striatal MSNs. VP glutamatergic neurons preferentially receive innervation from D1 MSNs, whereas VP GABA neurons receive both D1 and D2 afferents (*50*). In this study, we found that the VTA-to-VP GABA pathway appears to convey similar information as VTA-to-D1 MSN DA inputs at the time of reward consumption but not during delivery of the cue. Activation of both these pathways that are temporally complementary to each other during a reward behavior could result in increased and/or prolonged VP activity, convergently increasing and/or maintaining motivation to work for reward. VTA-to-VP GABA activity may inhibit VP glutamatergic neurons and activate VP GABAergic neurons either via co-release of glutamate onto GABA cells or by inhibiting VP interneurons. GABAergic interneurons comprise a large proportion of neurons in the VP (*25*), with pallidal noncholinergic type II interneurons comprising 56% of VP cells (*52*). Therefore, it is possible that GABAergic inputs to VP may result in disinhibition of the structure by targeting these interneurons.

In conclusion, the current study provides a novel framework for understanding how VTA activity drives motivation to work for rewarding stimuli by coordinating the outputs of NAc and VP. First, VTA-to-VP GABA neurons respond to reward in a different pattern than VTA DA neurons, scaling with the value of reward and providing an invariant reward signal that could be important for calculating prediction errors. Second, VTA-to-VP GABA neurons increase their activity in response to reward delivery, which in turn recruits more VP neurons for reward seeking, increases motivation to obtain rewards, and therefore improves performance during reward-related tasks. Previous studies have shown that VTA GABA neurons are involved in behaviors relevant to drug addiction and withdrawal-related stress (*4*, *5*). We therefore speculate that activity of the VTA-to-VP GABA projection neurons may be increased when motivation is abnormally elevated during drug craving, but decreased during drug withdrawal, depression, and other depressive disorders when motivation is impaired. Therefore, VTA GABA signaling could be a novel target in treatment of these disorders.

MATERIALS AND METHODS

Animals

Male and female GAD65-IRES-Cre mice (GAD65-Cre; 5 to 10 months, The Jackson Laboratory) and Cre^+/GFP^+ F1 derived from GAD65-Cre × GAD67-GFP (*53*) were group-housed on a 12:12-hour light-dark cycle with ad libitum food and water. Procedures were approved by the Yale University Institutional Animal Care and Use Committee and were in accordance with the National Institutes of Health (NIH) *Guide for Care and Use of Laboratory Animals*.

Surgery

For electrophysiological recordings and behavior experiments, GAD65-Cre mice were infused with AAV2-EF1a-DIO-hChR2(H134R)-eYFP (UNC Vector Core) in the VTA, as previously described (*20*). Coordinates for VTA infusions were, from bregma, [anterior-posterior (AP): −3.0 mm; medial-lateral (ML): ±0.4 mm; dorsal-ventral (DV): −4.6 mm]. For mice undergoing behavioral testing, customized bilateral cannulae (Doric Lenses, Canada) were implanted in VP (AP: +0.2; ML: ±1.2; DV: −4.5). Before electrophysiological recording or behavioral tests, mice were allowed to recover for >21 days. A recombinant, transsynaptic HSV (H129ΔTK-TT) for anterograde transsynaptic tracing (*26*) was injected unilaterally into the VTA (AP: −3.0; ML: −0.4; DV: −4.6). Mice were monitored daily, and brains were harvested at 96 hours after surgery. For fiber photometry, GAD65-Cre mice were infused with pGP-AAV1-syn-FLEX-jGCaMP7s-WPRE (Addgene, plasmid no. 104491) in the right VTA (AP: −3.0; ML: −0.4; DV: −4.6). To measure calcium activities in VTA GABA neuronal terminals projected in the VP, a mono fiber-optic cannula (Doric Lenses, Canada) was implanted above the right VP (AP: +0.2; ML: −1.2; DV: −4.5). For DREADD studies, injection of AAV8 Ef1a-fDIO-DREADD Gq-mCherry into the VTA (AP: −3.0; ML: −0.4; DV: −4.6) and injection of retrograde HSV-hEF1α-LS1L-flpo (RN433) or HSV-hEF1α-LS1L-BFP-flpo (RN434; MIT vector core) into the VP (AP: +0.2; ML: −1.2; DV: −5.2 to −4.6) were made on the same side. For in vivo calcium imaging, a 1:1 mixture of HSV-hEF1α-LS1L-flpo and AAV1-Syn-GCaMP6s-WPRE-SV40 (Penn Vector Core) was infused into the VP. Two weeks later, a lens probe (Inscopix; PN:100-002171) was implanted targeting VP (AP: +0.2; ML: −1.15; DV: −4.6). After an additional 2-week recovery, a baseplate for attaching the nVista microscope (Inscopix Inc.) was mounted over the lens. Last, a head plate was mounted behind the baseplate for head fixation during behavioral tasks (*54*).

Immunostaining

For neuroanatomical tracing and post hoc verification of placement, brains were sectioned to 50-μm-thick sagittal or coronal slices. Immunohistochemical staining was described in (*20*). Briefly, slices were blocked and incubated in primary antibody solutions overnight at 4°C. For double or triple labeling, slices were incubated in solutions containing multiple primary antibodies raised in different host species. Next, slices were incubated with secondary antibodies for 2 hours and then mounted onto glass slides for imaging. Antibodies and sources are listed in table S1.

Acute brain slices and electrophysiology

Mice for slice physiology studies were transcardially perfused with ice-cold, oxygenated artificial cerebrospinal fluid [ACSF; containing 125 mM NaCl, 26 mM $NaHCO_3$, 10 mM glucose, 2.3 mM KCl, 1.26 mM KH_2PO_4, 2 mM $CaCl_2$, and 1 mM $MgSO_4$ (pH 7.4)] for harvesting brains, which were immediately transferred to ice-cold, oxygenated ACSF. Brains were cut on a vibratome into 300-μm sagittal slices. Acute slices were incubated in a holding chamber with protective ACSF containing 5 mM kynurenic acid at 37°C for 30 min and then moved to and maintained at room temperature. All measurements were performed at room temperature, as described in (*55*). Whole-cell recordings were made nonselectively from visually identified neurons in the VP or in YFP-expressing neurons in the VTA for measuring systematic delay. Electrical signals were amplified with Multiclamp 700B and digitized with Digidata 1440A (Molecular Devices LLC). Intracellular solution contains 145 mM KCl, 2 mM $MgCl_2$, 3 mM Na_2–adenosine triphosphate (ATP), 0.3 mM Na_2–guanosine triphosphate (GTP), 1.1 mM K_2-EGTA, and 10 mM Hepes (pH 7.3). During recording, blue light pulses (10 ms, 1 Hz) were delivered to the recording chamber from a 465-nm light-emitting diode (LED) for optical stimulation. Only those recordings with stable series resistance (<30 megohms) were analyzed. For pharmacology, PTX (Abcam), CNQX (Abcam), and CNO [National Institute of Neurological Disorders and Stroke (NINDS)] were dissolved in ACSF at 5× final concentration and carefully

pipetted into the recording chamber against the wall. Electrical recordings were analyzed using Clampfit10 (Molecular Devices, Sunnyvale, CA) and filtered with Gaussian low-pass filter (500 Hz cutoff) before measurements.

Fiber photometry

The methods were adapted from (*56*) to measure in vivo calcium signals as fractional changes of fluorescence (d*F*/*F*), using a standard 2-lenses-1-site 405/465-nm fiber photometry system. The console controlled two connectorized LEDs (CLEDs; 405 nm modulated at 208 Hz and 465 nm modulated at 572 Hz). Each CLED was connected to a five-port Fluorescence MiniCube (FMC5_AE(405)_AF(420-450)_E1(460–490)_F1 (500–550)_S). The F1 (500–550 nm) MiniCube port was connected to the photoreceiver (AC low mode, New Focus 2151 Visible Femtowatt Photoreceiver, New Focus, CA) via a fiber optic adapter that was finally connected back to the fiber photometry console. A pigtailed fiber optic rotary joint connected the MiniCube and the patch cord to deliver and receive lights in a freely moving mouse through an implanted optical fiber. Signals were recorded using Doric Neuroscience Studio (V 5.3.3.14) via the Lock-In demodulation mode with a sampling rate of 12.0 kS/s. Data were decimated by a factor of 100 and saved as a comma-separated file. For the preprocessing of raw data, baseline fluorescence (*F*0) was calculated using a first-order least mean squares regression across the entire recording, and change in fluorescence (d*F*) was calculated as the difference between the recording and *F*0. d*F*/*F* for the reference (405 nm) channel was subtracted from the signal (465 nm) channel to remove movement artifacts and then *z*-scored. Traces were adjusted to a peri-event baseline by subtracting the average signal from 10 to 5 s before an event. Graphs were generated in MATLAB (2020b) by plotting data 10 s before and after an event (nosepoke, US retrieval, or cue onset). Heatmaps were generated by aligning to magazine entry and plotting the 10 s preceding and 10 s following the entry on a color scale map. AUC was calculated in MATLAB by performing numerical integration via the trapezoidal method for each peak from magazine entry to 5 s after the entry.

One caveat to note is that using the tools used in this study, we cannot fully separate afferents impinging on the VP from en passant fibers to the NAc. However, in mature axons, activity-dependent calcium influx mainly happens at presynaptic terminals through calcium channels and weakly at nodes through sodium channels (*57*–*59*). Therefore, compared to strong calcium signals in the axon terminals ending in the VP, the signals from sporadic nodes in the en passant fibers from VTA to NAc are likely to be weak and would be more difficult to detect. Nevertheless, it is possible that en passant fibers to the NAc might contribute to photometry signals to a limited extent.

Behavioral testing

Behavioral experiments were conducted as previously described (*56*). Commands and data collection were controlled with Med-PC IV software. Commanding codes are available upon request. Across behavioral training and testing, mice were food-restricted with body weight maintained at 90% of baseline. Briefly, mice were first trained following an FR1 schedule in a daily 60-min session. A nosepoke in the "active," LED-lit aperture triggered reward (Ensure Plus, Abbott; ~24 μl over 2 s) delivery in the magazine. Mice that earned ≥30 rewards in the last session were randomized and underwent injection of pGP-AAV-syn-FLEX-jGCaMP7s-WPRE for fiber photometry or injection of AAV2-EF1a-DIO-hChR2(H134R)-eYFP for behavioral testing. Recovery was allowed for >3 weeks before further experiments.

During CRT training, a speaker in each cabinet delivered tones (1 s, 70 dB) on a random time intertrial interval schedule of 30 s (RT-30). Following each tone, a 5-s window of reward availability was assigned, indicated by LED light in the active aperture. During this time window, a nosepoke in the active aperture triggered a reward (~48 μl over 4 s). For fiber photometry, a Transistor-transistor logic (TTL) pulse was used to synchronize behavioral and fluorescent recordings at the beginning of each session, and then the fluorescence recordings were kept for whole session or 60 min, whichever is shorter. For optogenetic stimulation, a 5-s train of blue light pulses (10 ms, 20 Hz, 465 nm; on-site end power of 90 to 100 mW/mm^2) was simultaneously delivered to the VP through bilateral light cannulae during each 5-s window of reward availability. A training session terminated after 180 min or once 30 cue + reward presentations were delivered. For CR testing, magazines were removed and three apertures were placed at the opposite side. One LED-lit aperture was assigned as active aperture. A nosepoke in active aperture resulted in cue and dipper presentation in the absence of reward. Active aperture responding was on an FR1 schedule for the first 10 nosepokes, followed by a variable-ratio 3 schedule.

PR testing was conducted in chambers with the same settings as FR1 training following an exponential progression derived from the formula $(5 \times e^{0.2n}) - 5$, as: 1, 2, 4, 6, 9, 12, 15, 20, 25, 32, 40, … (*60*). Each reward was set as a size of ~48 μl of Ensure over 4 s. For fiber photometry, a TTL pulse was used to synchronize behavioral and fluorescent recordings at the beginning of each session, and then the fluorescence recordings were kept for 60 min. For optogenetic stimulation, the same 5-s train of blue light pulses as that in CRT was delivered every 30 s. Each PR session was terminated when a mouse failed to nosepoke for 5 min. "Breakpoint" was defined as the time when mice stop nosepoke for ≥ 5 min and was measured as the total number of nosepokes achieved up to the final reinforcer.

In vivo calcium imaging in head-fixed, sucrose-seeking mice

A self-paced instrumental sucrose-seeking task was adapted from (*32*). Mice were water-deprived before training and throughout task sessions, while they obtained all fluid from extended licking. On the behavioral rig, mice were head-fixed but free to walk atop a rotating disk. The mice learned to earn drops of fluid (~4 μl) by licking a composite spout that delivers water (0%) and sucrose (3 and 10%) solutions independently. The tri-viral infected mice were first trained on an FR1 schedule to seek 3% sucrose for 2 days and then on an FR10-FI5 schedule (Fig. 5E) for 4 days. The 5-s timeout is to separate motivated licks from consummatory ones. Completing a first FR10 initiates a 60-s time block, during which a single type of fluid was provided. From block to block, the fluid type changes following 0% → 3% → 10% → 3%. Fluid delivery and licks were controlled and monitored using Presentation software (Neurobehavioral Systems) through two independent data acquisition boards (USB-201, Measurement Computing).

On the day of an imaging session, 30 min before imaging, the mice were injected intraperitoneally with vehicle (dimethyl sulfoxide:saline = 1:4, 10 μl/10 g) or CNO (2 mg/ml) in the following order: vehicle, CNO, no injection, vehicle, CNO, over 5 days. Thirty minutes later, the mice were head-fixed on the behavior rig and the microscope (Inscopix) was attached to the implanted lens. The microscope was adjusted so that the fields of view were consistent across imaging

days by observing the pattern of fluorescence and blood vessels. nVista HD acquisition software was used for imaging. TTL pulses from Presentation software were used for post hoc alignment of imaging with behavioral data. After 3 min of baseline imaging, the sucrose-seeking task commenced. Thirty minutes later, the imaging was terminated, and the mice continued the task to obtain fluid for the day until satiated.

All image processing was performed using a combination of Mosaic (version 1.2; Inscopix) and custom scripts in MATLAB (MathWorks Inc.). Briefly, the movies from all imaging sessions were cropped, temporally down-sampled (5 Hz), concatenated, and motion-corrected. We then used a Principal Component Analysis/Independent Component Analysis algorithm to identify spatial filters corresponding to putative neurons. The filters and their corresponding fluorescence traces were then manually inspected to obtain the final set of neurons for analysis: roughly circular structures of diameter ~10 μm and good (>3) signal-to-noise ratio as identified by peaks of fluorescence relative to SD of baseline noise. The raw fluorescence traces for each neuron were used to calculate the fractional change in fluorescence (dF/F), which were then aligned with the behavioral TTL pulses for calculation of event-related changes in dF/F as determined by (dF/F at 1 s after event) − (dF/F at 1 s before event). The significance of the change in dF/F of each cell was analyzed using Wilcoxon signed-rank test, and those cells with $P < 0.05$ were used for testing the significances of the vehicle and CNO treatments.

SUPPLEMENTARY MATERIALS

Supplementary material for this article is available at https://science.org/doi/10.1126/sciadv.abm5217

View/request a protocol for this paper from *Bio-protocol*.

REFERENCES AND NOTES

1. M. Morales, E. B. Margolis, Ventral tegmental area: Cellular heterogeneity, connectivity and behaviour. *Nat. Rev. Neurosci.* **18**, 73–85 (2017).
2. W. Schultz, P. Dayan, P. R. Montague, A neural substrate of prediction and reward. *Science* **275**, 1593–1599 (1997).
3. R. A. Wise, Dopamine, learning and motivation. *Nat. Rev. Neurosci.* **5**, 483–494 (2004).
4. S. Tolu, R. Eddine, F. Marti, V. David, M. Graupner, S. Pons, M. Baudonnat, M. Husson, M. Besson, C. Reperant, J. Zemdegs, C. Pagès, Y. A. H. Hay, B. Lambolez, J. Caboche, B. Gutkin, A. M. Gardier, J. P. Changeux, P. Faure, U. Maskos, Co-activation of VTA DA and GABA neurons mediates nicotine reinforcement. *Mol. Psychiatry* **18**, 382–393 (2013).
5. C. Bouarab, B. Thompson, A. M. Polter, VTA GABA neurons at the interface of stress and reward. *Front. Neural Circuits* **13**, 78 (2019).
6. K. T. Wakabayashi, M. Feja, A. N. Baindur, M. J. Bruno, R. V. Bhimani, J. Park, K. Hausknecht, R. Y. Shen, S. Haj-Dahmane, C. E. Bass, Chemogenetic activation of ventral tegmental area GABA neurons, but not mesoaccumbal GABA terminals, disrupts responding to reward-predictive cues. *Neuropsychopharmacology* **44**, 372–380 (2019).
7. J. Y. Cohen, S. Haesler, L. Vong, B. B. Lowell, N. Uchida, Neuron-type-specific signals for reward and punishment in the ventral tegmental area. *Nature* **482**, 85–88 (2012).
8. M. C. Creed, N. R. Ntamati, K. R. Tan, VTA GABA neurons modulate specific learning behaviors through the control of dopamine and cholinergic systems. *Front. Behav. Neurosci.* **8**, 8 (2014).
9. M. T. C. Brown, K. R. Tan, E. C. O'Connor, I. Nikonenko, D. Muller, C. Lüscher, Ventral tegmental area GABA projections pause accumbal cholinergic interneurons to enhance associative learning. *Nature* **492**, 452–456 (2012).
10. R. Al-Hasani, R. Gowrishankar, G. P. Schmitz, C. E. Pedersen, D. J. Marcus, S. E. Shirley, T. E. Hobbs, A. J. Elerding, S. J. Renaud, M. Jing, Y. Li, V. A. Alvarez, J. C. Lemos, M. R. Bruchas, Ventral tegmental area GABAergic inhibition of cholinergic interneurons in the ventral nucleus accumbens shell promotes reward reinforcement. *Nat. Neurosci.* **24**, 1414–1428 (2021).
11. S. C. Steffensen, R. S. Lee, S. H. Stobbs, S. J. Henriksen, Responses of ventral tegmental area GABA neurons to brain stimulation reward. *Brain Res.* **906**, 190–197 (2001).
12. A. Eban-Rothschild, J. C. Borniger, G. Rothschild, W. J. Giardino, J. G. Morrow, L. de Lecea, Arousal state-dependent alterations in VTA-GABAergic neuronal activity. *eNeuro* **7**, ENEURO.0356-19.2020 (2020).
13. C. W. Berridge, A. F. Arnsten, Psychostimulants and motivated behavior: Arousal and cognition. *Neurosci. Biobehav. Rev.* **37**, 1976–1984 (2013).
14. R. G. Nair-Roberts, S. D. Chatelain-Badie, E. Benson, H. White-Cooper, J. P. Bolam, M. A. Ungless, Stereological estimates of dopaminergic, GABAergic and glutamatergic neurons in the ventral tegmental area, substantia nigra and retrorubral field in the rat. *Neuroscience* **152**, 1024–1031 (2008).
15. R. van Zessen, J. L. Phillips, E. A. Budygin, G. D. Stuber, Activation of VTA GABA neurons disrupts reward consumption. *Neuron* **73**, 1184–1194 (2012).
16. K. R. Tan, C. Yvon, M. Turiault, J. J. Mirzabekov, J. Doehner, G. Labouèbe, K. Deisseroth, K. M. Tye, C. Lüscher, GABA neurons of the VTA drive conditioned place aversion. *Neuron* **73**, 1173–1183 (2012).
17. Y. Takata, Y. Oishi, X. Z. Zhou, E. Hasegawa, K. Takahashi, Y. Cherasse, T. Sakurai, M. Lazarus, Sleep and wakefulness are controlled by ventral medial midbrain/pons GABAergic neurons in mice. *J. Neurosci.* **38**, 10080–10092 (2018).
18. X. Yu, W. Ba, G. Zhao, Y. Ma, E. C. Harding, L. Yin, D. Wang, H. Li, P. Zhang, Y. Shi, R. Yustos, A. L. Vyssotski, H. Dong, N. P. Franks, W. Wisden, Dysfunction of ventral tegmental area GABA neurons causes mania-like behavior. *Mol. Psychiatry* **26**, 5213–5228 (2020).
19. W. Schultz, Neuronal reward and decision signals: From theories to data. *Physiol. Rev.* **95**, 853–951 (2015).
20. S. R. Taylor, S. Badurek, R. J. Dileone, R. Nashmi, L. Minichiello, M. R. Picciotto, GABAergic and glutamatergic efferents of the mouse ventral tegmental area. *J. Comp. Neurol.* **522**, 3308–3334 (2014).
21. J. H. Yoo, V. Zell, N. Gutierrez-Reed, J. Wu, R. Ressler, M. A. Shenasa, A. B. Johnson, K. H. Fife, L. Faget, T. S. Hnasko, Ventral tegmental area glutamate neurons co-release GABA and promote positive reinforcement. *Nat. Commun.* **7**, 13697 (2016).
22. Y. M. Kupchik, R. M. Brown, J. A. Heinsbroek, M. K. Lobo, D. J. Schwartz, P. W. Kalivas, Coding the direct/indirect pathways by D1 and D2 receptors is not valid for accumbens projections. *Nat. Neurosci.* **18**, 1230–1232 (2015).
23. R. J. Smith, M. K. Lobo, S. Spencer, P. W. Kalivas, Cocaine-induced adaptations in D1 and D2 accumbens projection neurons (a dichotomy not necessarily synonymous with direct and indirect pathways). *Curr. Opin. Neurobiol.* **23**, 546–552 (2013).
24. K. S. Smith, A. J. Tindell, J. W. Aldridge, K. C. Berridge, Ventral pallidum roles in reward and motivation. *Behav. Brain Res.* **196**, 155–167 (2009).
25. D. H. Root, R. I. Melendez, L. Zaborszky, T. C. Napier, The ventral pallidum: Subregion-specific functional anatomy and roles in motivated behaviors. *Prog. Neurobiol.* **130**, 29–70 (2015).
26. L. Lo, D. J. Anderson, A cre-dependent, anterograde transsynaptic viral tracer for mapping output pathways of genetically marked neurons. *Neuron* **72**, 938–950 (2011).
27. C. P. Bengtson, P. B. Osborne, Electrophysiological properties of cholinergic and noncholinergic neurons in the ventral pallidal region of the nucleus basalis in rat brain slices. *J. Neurophysiol.* **83**, 2649–2660 (2000).
28. D. H. Root, C. A. Mejias-Aponte, S. Zhang, H. L. Wang, A. F. Hoffman, C. R. Lupica, M. Morales, Single rodent mesohabenular axons release glutamate and GABA. *Nat. Neurosci.* **17**, 1543–1551 (2014).
29. N. R. Ntamati, C. Luscher, VTA projection neurons releasing GABA and glutamate in the dentate gyrus. *eNeuro* **3**, ENEURO.0137-16.2016 (2016).
30. A. Fujimoto, Y. Hori, Y. Nagai, E. Kikuchi, K. Oyama, T. Suhara, T. Minamimoto, Signaling incentive and drive in the primate ventral pallidum for motivational control of goal-directed action. *J. Neurosci.* **39**, 1793–1804 (2019).
31. D. Ottenheimer, J. M. Richard, P. H. Janak, Ventral pallidum encodes relative reward value earlier and more robustly than nucleus accumbens. *Nat. Commun.* **9**, 4350 (2018).
32. F. Barthas, M. Y. Hu, M. J. Siniscalchi, F. Ali, Y. S. Mineur, M. R. Picciotto, A. C. Kwan, Cumulative effects of social stress on reward-guided actions and prefrontal cortical activity. *Biol. Psychiatry* **88**, 541–553 (2020).
33. G. J. Mogenson, D. L. Jones, C. Y. Yim, From motivation to action: Functional interface between the limbic system and the motor system. *Prog. Neurobiol.* **14**, 69–97 (1980).
34. V. Coizet, E. Comoli, G. W. Westby, P. Redgrave, Phasic activation of substantia nigra and the ventral tegmental area by chemical stimulation of the superior colliculus: An electrophysiological investigation in the rat. *Eur. J. Neurosci.* **17**, 28–40 (2003).
35. W. Hodos, Progressive ratio as a measure of reward strength. *Science* **134**, 943–944 (1961).
36. B. A. Baldo, R. A. Daniel, C. W. Berridge, A. E. Kelley, Overlapping distributions of orexin/hypocretin- and dopamine-beta-hydroxylase immunoreactive fibers in rat brain regions mediating arousal, motivation, and stress. *J. Comp. Neurol.* **464**, 220–237 (2003).
37. D. Gagnon, M. Parent, Distribution of VGLUT3 in highly collateralized axons from the rat dorsal raphe nucleus as revealed by single-neuron reconstructions. *PLOS ONE* **9**, e87709 (2014).

38. L. Zaborszky, R. P. Gaykema, D. J. Swanson, W. E. Cullinan, Cortical input to the basal forebrain. *Neuroscience* **79**, 1051–1078 (1997).
39. M. S. Turner, A. Lavin, A. A. Grace, T. C. Napier, Regulation of limbic information outflow by the subthalamic nucleus: Excitatory amino acid projections to the ventral pallidum. *J. Neurosci.* **21**, 2820–2832 (2001).
40. I. Ubeda-Bañon, A. Novejarque, A. Mohedano-Moriano, P. Pro-Sistiaga, C. de la Rosa-Prieto, R. Insausti, F. Martinez-Garcia, E. Lanuza, A. Martinez-Marcos, Projections from the posterolateral olfactory amygdala to the ventral striatum: Neural basis for reinforcing properties of chemical stimuli. *BMC Neurosci.* **8**, 103 (2007).
41. A. J. Granger, M. L. Wallace, B. L. Sabatini, Multi-transmitter neurons in the mammalian central nervous system. *Curr. Opin. Neurobiol.* **45**, 85–91 (2017).
42. D. H. Root, D. J. Barker, D. J. Estrin, J. A. Miranda-Barrientos, B. Liu, S. Zhang, H. L. Wang, F. Vautier, C. Ramakrishnan, Y. S. Kim, L. Fenno, K. Deisseroth, M. Morales, Distinct signaling by ventral tegmental area glutamate, GABA, and combinatorial glutamate-GABA neurons in motivated behavior. *Cell Rep.* **32**, 108094 (2020).
43. D. J. Ottenheimer, B. A. Bari, E. Sutlief, K. M. Fraser, T. H. Kim, J. M. Richard, J. Y. Cohen, P. H. Janak, A quantitative reward prediction error signal in the ventral pallidum. *Nat. Neurosci.* **23**, 1267–1276 (2020).
44. Y. M. Vachez, J. R. Tooley, K. Abiraman, B. Matikainen-Ankney, E. Casey, T. Earnest, L. M. Ramos, H. Silberberg, E. Godynyuk, O. Uddin, L. Marconi, C. E. le Pichon, M. C. Creed, Ventral arkypallidal neurons inhibit accumbal firing to promote reward consumption. *Nat. Neurosci.* **24**, 379–390 (2021).
45. K. S. Smith, K. C. Berridge, The ventral pallidum and hedonic reward: Neurochemical maps of sucrose "liking" and food intake. *J. Neurosci.* **25**, 8637–8649 (2005).
46. T. Shimura, H. Imaoka, T. Yamamoto, Neurochemical modulation of ingestive behavior in the ventral pallidum. *Eur. J. Neurosci.* **23**, 1596–1604 (2006).
47. R. D. Palmiter, Dopamine signaling in the dorsal striatum is essential for motivated behaviors: Lessons from dopamine-deficient mice. *Ann. N. Y. Acad. Sci.* **1129**, 35–46 (2008).
48. K. S. Smith, K. C. Berridge, Opioid limbic circuit for reward: Interaction between hedonic hotspots of nucleus accumbens and ventral pallidum. *J. Neurosci.* **27**, 1594–1605 (2007).
49. M. Stephenson-Jones, C. Bravo-Rivera, S. Ahrens, A. Furlan, X. Xiao, C. Fernandes-Henriques, B. Li, Opposing contributions of GABAergic and glutamatergic ventral pallidal neurons to motivational behaviors. *Neuron* **105**, 921–933.e5 (2020).
50. J. A. Heinsbroek, A.-C. Bobadilla, E. Dereschewitz, A. Assali, R. M. Chalhoub, C. W. Cowan, P. W. Kalivas, Opposing regulation of cocaine seeking by glutamate and GABA neurons in the ventral pallidum. *Cell Rep.* **30**, 2018–2027.e3 (2020).
51. J. Tooley, L. Marconi, J. B. Alipio, B. Matikainen-Ankney, P. Georgiou, A. V. Kravitz, M. C. Creed, Glutamatergic ventral pallidal neurons modulate activity of the habenula-tegmental circuitry and constrain reward seeking. *Biol. Psychiatry* **83**, 1012–1023 (2018).
52. A. Nambu, R. Llinas, Morphology of globus pallidus neurons: Its correlation with electrophysiology in guinea pig brain slices. *J. Comp. Neurol.* **377**, 85–94 (1997).
53. N. Tamamaki, Y. Yanagawa, R. Tomioka, J. I. Miyazaki, K. Obata, T. Kaneko, Green fluorescent protein expression and colocalization with calretinin, parvalbumin, and somatostatin in the GAD67-GFP knock-in mouse. *J. Comp. Neurol.* **467**, 60–79 (2003).
54. M. J. Siniscalchi, V. Phoumthipphavong, F. Ali, M. Lozano, A. C. Kwan, Fast and slow transitions in frontal ensemble activity during flexible sensorimotor behavior. *Nat. Neurosci.* **19**, 1234–1242 (2016).
55. W. L. Zhou, X. B. Gao, M. R. Picciotto, Acetylcholine acts through nicotinic receptors to enhance the firing rate of a subset of hypocretin neurons in the mouse hypothalamus through distinct presynaptic and postsynaptic mechanisms. *eNeuro* **2**, ENEURO.0052-14.2015 (2015).
56. R. B. Crouse, K. Kim, H. M. Batchelor, E. M. Girardi, R. Kamaletdinova, J. Chan, P. Rajebhosale, S. T. Pittenger, L. W. Role, D. A. Talmage, M. Jing, Y. Li, X. B. Gao, Y. S. Mineur, M. R. Picciotto, Acetylcholine is released in the basolateral amygdala in response to predictors of reward and enhances the learning of cue-reward contingency. *eLife* **9**, e57335 (2020).
57. F. Ali, A. C. Kwan, Interpreting in vivo calcium signals from neuronal cell bodies, axons, and dendrites: A review. *Neurophotonics* **7**, 011402 (2020).
58. A. Battefeld, M. A. Popovic, S. I. de Vries, M. H. P. Kole, High-frequency microdomain Ca^{2+} transients and waves during early myelin internode remodeling. *Cell Rep.* **26**, 182–191.e5 (2019).
59. N. A. Hanemaaijer, M. A. Popovic, X. Wilders, S. Grasman, O. Pavón Arocas, M. H. P. Kole, Ca^{2+} entry through Na_V channels generates submillisecond axonal Ca^{2+} signaling. *eLife* **9**, e54566 (2020).
60. J. F. Rickard, S. Body, Z. Zhang, C. M. Bradshaw, E. Szabadi, Effect of reinforcer magnitude on performance maintained by progressive-ratio schedules. *J. Exp. Anal. Behav.* **91**, 75–87 (2009).
61. H. R. Kissileff, M. Herzog, Progressive ratio (PR) schedules and the sipometer: Do they measure wanting, liking, and/or reward? A tribute to Anthony Sclafani and Karen Ackroff. *Appetite* **122**, 44–50 (2018).
62. P. Skjoldager, P. J. Pierre, G. Mittleman, Reinforcer magnitude and progressive ratio responding in the rat—Effects of increased effort, prefeeding, and extinction. *Learn Motiv.* **24**, 303–343 (1993).
63. J. Olds, Self-stimulation of the brain; Its use to study local effects of hunger, sex, and drugs. *Science* **127**, 315–324 (1958).
64. G. M. Alexander, S. C. Rogan, A. I. Abbas, B. N. Armbruster, Y. Pei, J. A. Allen, R. J. Nonneman, J. Hartmann, S. S. Moy, M. A. Nicolelis, J. O. McNamara, B. L. Roth, Remote control of neuronal activity in transgenic mice expressing evolved G protein-coupled receptors. *Neuron* **63**, 27–39 (2009).

Acknowledgments: We thank A. Iwasaki and M. Linehan for providing the biosafety level 2 facility and technical support for HSV (H129ΔTK-TT) experiments. We thank X.-B. Gao and S. Antic for intellectual discussions. We thank the Center for Neuroanatomy with Neurotropic Viruses, Pittsburgh, PA and NIH Virus Center grant no. P40 OD010996 for providing HSV constructs (H129ΔTK-TT). We also thank NINDS Rapid Access to Investigative Drugs Stock for providing clozapine *N*-oxide. **Funding:** This study was supported by grants DA014241, DA050986, and DA036151 from the NIH. This work was funded in part by the State of Connecticut, Department of Mental Health and Addiction Services, but this publication does not express the views of the Department of Mental Health and Addiction Services or the State of Connecticut. **Author contributions:** W.-L.Z. and M.R.P. conceived the project and designed the studies. W.-L.Z. carried out and analyzed anatomical, behavioral, and electrophysiological studies. W.-L.Z., K.K., and M.R.P. designed, and K.K. carried out and analyzed fiber photometry experiments. W.-L.Z., F.A., and A.C.K. designed, carried out, and analyzed in vivo calcium imaging experiments. S.T.P., C.A.C., and Y.S.M. contributed to design of behavioral studies. C.R. and K.D. designed, generated, packaged, and purified pAAV-EF1a-fDIO-hM3D(Gq)-mCherry. All authors discussed the results and commented on the manuscript. **Competing interests:** The authors declare that they have no competing interests. **Data and materials availability:** All data needed to evaluate the conclusions in the paper are present in the paper and/or the Supplementary Materials.

Submitted 22 September 2021
Accepted 1 September 2022
Published 19 October 2022
10.1126/sciadv.abm5217

ScienceAdvances

Activity of a direct VTA to ventral pallidum GABA pathway encodes unconditioned reward value and sustains motivation for reward

Wen-Liang ZhouKristen KimFarhan AliSteven T. PittengerCali A. CalarcoYann S. MineurCharu RamakrishnanKarl DeisserothAlex C. KwanMarina R. Picciotto

Sci. Adv., 8 (42), eabm5217. • DOI: 10.1126/sciadv.abm5217

Science Advances (ISSN) is published by the American Association for the Advancement of Science. 1200 New York Avenue NW, Washington, DC 20005. The title *Science Advances* is a registered trademark of AAAS.